Simplified Dual-Frequency Wilkinson Power Divider with Enhanced Out-of-Band Performance for Millimeter-Wave Applications

Walid Zahra* **and Tarek Djerafi**

Abstract—A dual-band Wilkinson power divider covering comprehensive frequency ratios with improved Out-of-Band rejection is proposed with the use of only a resistor. In millimeter-wave range, the established lumped element based design with a wide range of frequency ratio suffers from the nonexistence of tiny required values and the difficulties of integrating them in the proposed designs. To tackle some of the more common millimeter-wave frequency bands challenges, the RLC is substituted in the design by transmission lines and a single resistor. The design parameters and rules are derived theoretically using even/odd mode analysis, and it takes into consideration the Out-of-Band performance. For validation, three different dual-frequency bands are studied (5.8–28 GHz, 20–35 GHz, and 28–35 GHz). The simulated and experimental results exhibit all the advantages of the proposed Wilkinson power divider, succeeding in boosting multi-functional and multi-standard RF and mm-wave front-ends for communication systems.

1. INTRODUCTION

Wilkinson power divider/combiner (WPD) is a component with a wide range of applications in microwave communication systems. By definition, it has high isolation and low transmission loss [1], and conventionally operates around a single frequency band [2, 3]. However, emerging 5G technology highlights the need to cover sub-6 GHz and millimeter bands in parallel with current technologies such as 3G and 4G requiring systems and components to operate in two or more bands simultaneously [4–7].

For dual-band Wilkinson power divider/ combiner (DBWPD) operation, different mechanisms such as open/short-circuited stubs, lumped-element components, or multi-section transformers have been used. The scheme presented in [2] consists of two transmission lines with the same impedance and a central stub. Operating frequencies with a limited frequency ratio > 1.7 and < 2.1 are achieved with an open stub circuit. For the short stub circuit > 2.0 and < 2.5 are attained. Cheng and Wong [3] proposed a design for a dual-band WPD based on two quarter-wave transmission lines and an open stub. The analysis suggests that the power divider operates at a frequency ratio ranging from 2.0 to 2.75, which can be constructed. Another approach is proposed by [8] with the use of two quarter-wavelength transmission lines and an open-circuited quarter-wavelength stub connecting to the input access and an isolation resistor. The two bands operate at limited frequency ratio ranging from 1.3 to 2.7. Wang et al. [9] determined unequal-enabled power division dual-band WPD consisting of two transmission lines with a parallel LC circuit at the midpoint between the two sections of the transmission lines. The range of lower and upper band frequency ratios discussed in [9] are from 1 to 7. In [10], the design consists of two sections of impedance transformers, and resistor, capacitor, and inductor in parallel that shunts the two output ports. The design operates over a wide range of frequency ratios (1 to 7).

In the context of 5G, the required frequency ratio range is large. In fact, the new generation of multi-functional systems will continue to work on traditional bands below 6 GHz and in mm-wave bands.

* Corresponding author: Walid Zahra (zahra.walid@inrs.com).
The authors are with the Institut National de la Recherche Scientifique INRS, Canada.

The WPD versions with RLC lumped element circuit which achieves the required ratio have several drawbacks. The lumped elements could cause many issues such as the parasitic effect, discontinuity, additional processes, lack of space, and coupling between the output ports. In addition, the required lumped elements values availability in the market, especially at mm-wave bands, is limited or even nonexistent. These and other issues are particularly evident when aiming to obtain high frequencies [11]. Moreover, most of the mentioned power divider designs suffer from poor out-of-band rejection. In fact, in the combining scenario, the unwanted band between the two operational frequencies is rejected. However, in the case of division, these power dividers show good matching and transmission coefficient not only at the expected bands but also at the band between them. This issue should be resolved to satisfy the strict nomination of dual-band divider/combiner. Some works, such as [12], make effort to improve Out-Of-Band rejection.

In this paper, a new topology is proposed by using four-section transmission lines and a resistor that substitutes the traditionally used lumped elements (R, L, and C). Resistors generally have the most stable values over broadband frequencies and are easier to find in the market for mm-wave range (as lumped element or with thin film process) [11]. The out-of-band rejection is considered in the selection of the two additional transmission lines. The new proposed design rules are provided based on even/odd mode analysis. To validate the concept, three prototypes are prepared with discretion of frequency ratio capability.

2. DUAL-BAND WILKINSON POWER DIVIDER WITH $R.L.C$

A schematic diagram of the proposed Wilkinson power divider, which realizes an equal power division at two arbitrary frequencies, is shown in Figure 1. In this design, part of the rules defined in the design are proposed by Wu et al. [10] in which a wider frequency ratio in the literature is conserved. Two sections of transmission line with characteristic impedance and length Z_1, l_1 and Z_2, l_2 are respectively used. Parallel lumped circuit of resistor R, inductor L, and capacitor C are shunting the output ports. This paper proposes the substitution of RLC lumped elements by only resistor r and transmission line with the characteristic impedance of Z_3 and Z_4 and the length of l_3 and l_4, respectively. In this section, the different rules and limitations of the design in the mm-wave are presented.
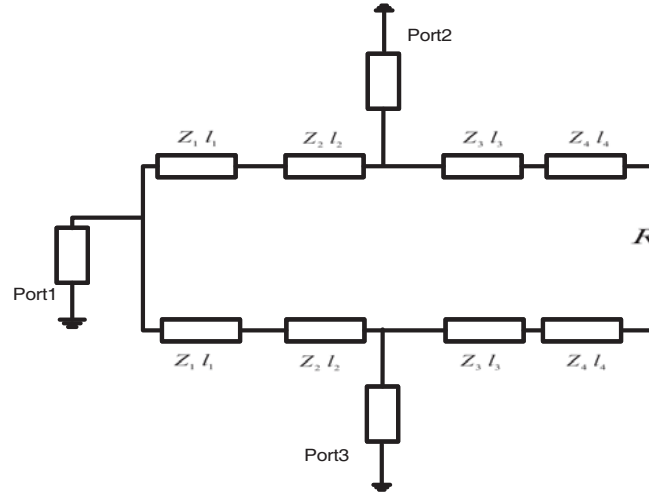

Figure 1. Proposed topology with resistance and two additional transmission lines.

2.1. Rules

The dual-band transformer rules are derived from [10, 13] considering : $Z_1, Z_2, \ell_1, \ell_2, R, L, C$

$$\ell_1 = \ell_2 = \frac{n\pi}{\beta_1 + \beta_2} \tag{1}$$

where n is an arbitrary integer, and β_1 and β_2 are applied to frequencies f_1 and f_2.

Consider α as:

$$\alpha = (\tan(\beta_1.\ell_1))^2 \tag{2}$$

The transmission lines impedances are defined as:

$$Z_2 = Z_0\sqrt{\frac{1}{2\alpha} + \sqrt{\frac{1}{(4\alpha)^2} + 2}} \tag{3}$$

$$Z_1 = \frac{2Z_0^2}{Z_2} \tag{4}$$

To find the unknowns L, C, parameters A and B are introduced

$$A = \frac{Z_2 - Z_1\tan(\beta_1\ell_1)^2}{Z_2(Z_1 + Z_2)\tan(\beta_1\ell_1)} \tag{5}$$

$$B = \frac{Z_2 - Z_1\tan(\beta_2\ell_1)2}{Z_2(Z_1 + Z_2)\tan(\beta_2\ell_1)} \tag{6}$$

$$C = \frac{\dfrac{B}{\omega_1} - \dfrac{A}{\omega_2}}{\dfrac{2\omega_2}{\omega_1} - \dfrac{2\omega_1}{\omega_2}} \tag{7}$$

$$L = \frac{\dfrac{2\omega_2}{\omega_1} - \dfrac{2\omega_1}{\omega_2}}{B\omega_1 - A\omega_2} \tag{8}$$

2.2. Frequency Ratio Study

The relation between m and n for the dual-band WPD that operates at f_1 and $m \times f_1$ is:

  (i) When the m value is greater than 1 and less than 3, $n =$1.
 (ii) When m is greater than $4(n-1)-1$ and less than $(4n-1)$, n is greater than or equal to 2.
(iii) The frequency ratio m equal to $4n-1$ is simply achievable with conventional WPD.

The values of Z_1 and Z_2 are studied to verify the feasible ratio range.

Figure 2 shows different frequency ratios correlated to Z_1 and Z_2 considering Z_0 equal to $50\,\Omega$. It is noticeable that frequency ratios 3 and 7 are achievable in conventional WPD. Other frequency ratios > 1 and ≤ 8 are realizable with values between 66 and $84\,\Omega$ for Z_1 and from 59.48 to $75.17\,\Omega$ for Z_2.

2.3. Design Examples

For concept validation, a design following rules in Eqs. (1) to (8) has been simulated using Advanced Design System (ADS2016). The design and simulation are done for a set of dual-frequencies: 2.4–5.8 GHz, 5.8–28 GHz, 20–35 GHz, and 28–35 GHz. Table 1 exhibits the ideal transmission line parameters and lumped element values for the initial design. Each dual-frequency design is simulated using the ideal transmission line without packaging consideration. For the bandwidth, the isolation is considered at 20 dB and return loss at 10 dB.

The simulation results are shown in Figure 3. In Figure 3(a), bandwidths about 0.6 GHz around 2.4 GHz, and 0.7 GHz at 5.8 GHz are achieved. For the second dual-frequency design (5.8–28 GHz),
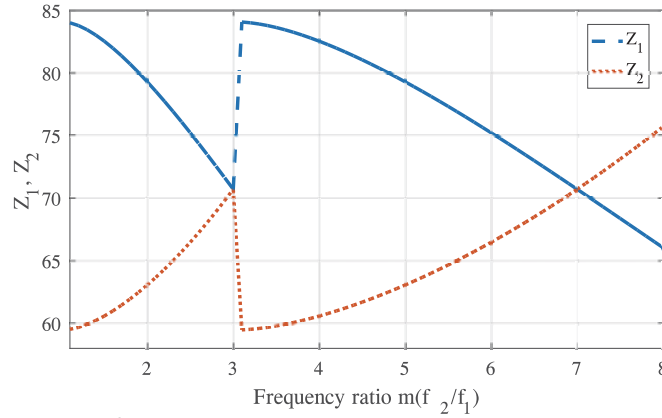
Figure 2. Frequency ratio m and Z_1, Z_2.

(a) 2.4-5.8 GHz

(b) 5.8-28 GHz
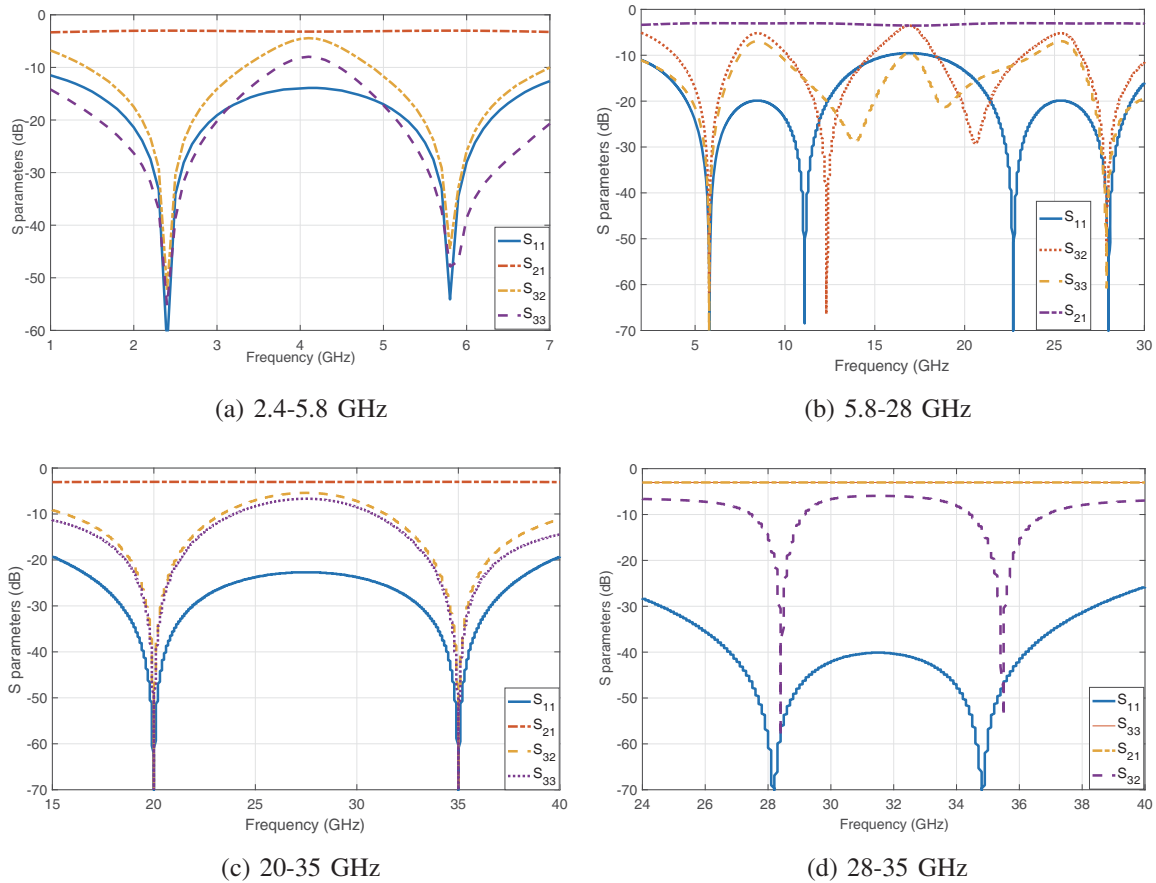
(c) 20-35 GHz

(d) 28-35 GHz

Figure 3. Ideal design (a) 2.4–5.8 GHz, (b) 5.8–28 GHz, (c) 20–35 GHz, (d) 28–35 GHz.

in Figure 3(b), bandwidths of 1.1 GHz at 5.8 GHz and 1.5 GHz at 28 GHz are achieved. In the third design (20–35 GHz), the results show good isolation with about 2 GHz bandwidth at both frequencies. The 28–35 GHz design result is illustrated in Figure 3(d). Its bandwidths are about 0.4 GHz at 28 GHz and 0.6 GHz at 35 GHz, and its reflection coefficient at port 1 shows one wide band between the two frequencies. Overall, it exhibits good matching at all the bands (28–35 GHz).

All simulation results in Figure 3 show poor Out-Of-Band rejection for the undesirable bands. Between the two targeted bands, the matching at port 1 is better than 10 dB while at ports 2 and 3 the matching is better than 6 dB.

Table 1. Frequency ratio and lumped elements values for different frequencies at the initial design.

f_1	f_2	f_0	Z_1	Z_2	θ_1,θ_2	R	L_{nH}	C_{pF}
2.4	5.8	4.1	75.9	65.8	52.6	100	14.6	0.12
5.8	28	16.9	79.9	62.5	61.7	100	3.36	0.05
20	35	27.5	81.0	61.6	65.4	100	0.4	0.09
28	35	31.5	83.6	59.7	80	100	0.04	0.61

2.4. mm-Wave Behavior

Advancing from 3G and 4G to 5G will add new opportunities. On the other hand, it will also add new challenges and hurdles. Millimeter-wave frequencies limitations for WPD are related to the transmission line, lumped elements, parasitic effects, and coupling. Transmission line length decreases with the decrease in wavelength for the same electrical length, whereas the width defined by the characteristic impedance remains constant. Consequently, the space framework of such a layout becomes inadequate when minimizing the length-to-width ratio. At the same time, the placement of lumped elements and the space between them make fabrication challenging [14]. Utilizing WPD in K-band frequencies or higher, the use of lumped elements raises many issues. Integrated resistors and other lumped elements become electrically large to be negligible. Elements dimension and space that is added to the physical layout should be taking into account [15]. Furthermore, problems dealing with the parasitic effect of both integrated or packaged resistors influences circuit performance. As higher frequencies are applied, obtaining the required values for capacitor and inductor becomes difficult because of their very small values. For that, their market availability is limited. Even though some values are available, placing and integrating them into the circuit is a challenging task.

As illustrated in Figure 4, the dimension of lumped elements is very small. Consequently, output branches of the power divider are placed close to each other which is in return causes coupling between them. Coupling between output ports dissipates power insertion and split.
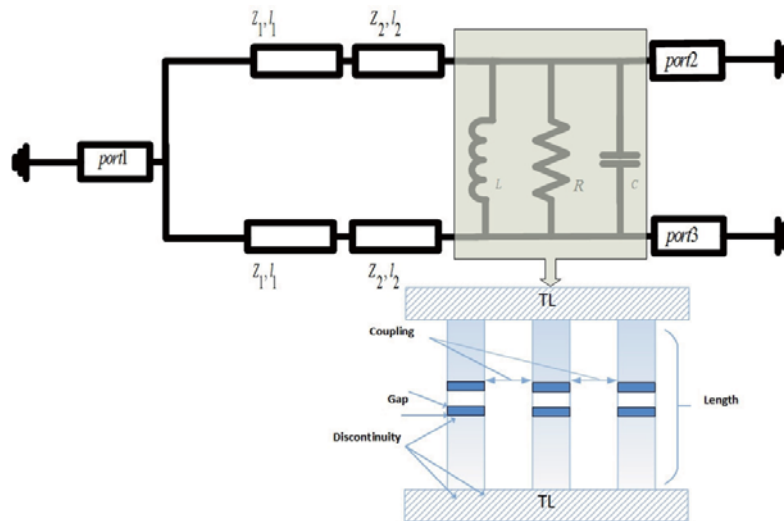

Figure 4. Proposed version with resistance and two additional transmission lines.

The effects on the performances can be seen in simulations in Figure 5 for the same dual frequencies illustrated in Figure 3, regarding packaging consideration. Characteristics added to the packaging are gap, coupling, and impedance discontinuity. The graph presented in Figure 5(a) shows that the simulated performances are in good agreement with the initial results (Figure 3(a)). The acceptable results are because the framework effects are negligible at lower frequencies. Figure 5(b) depicts that
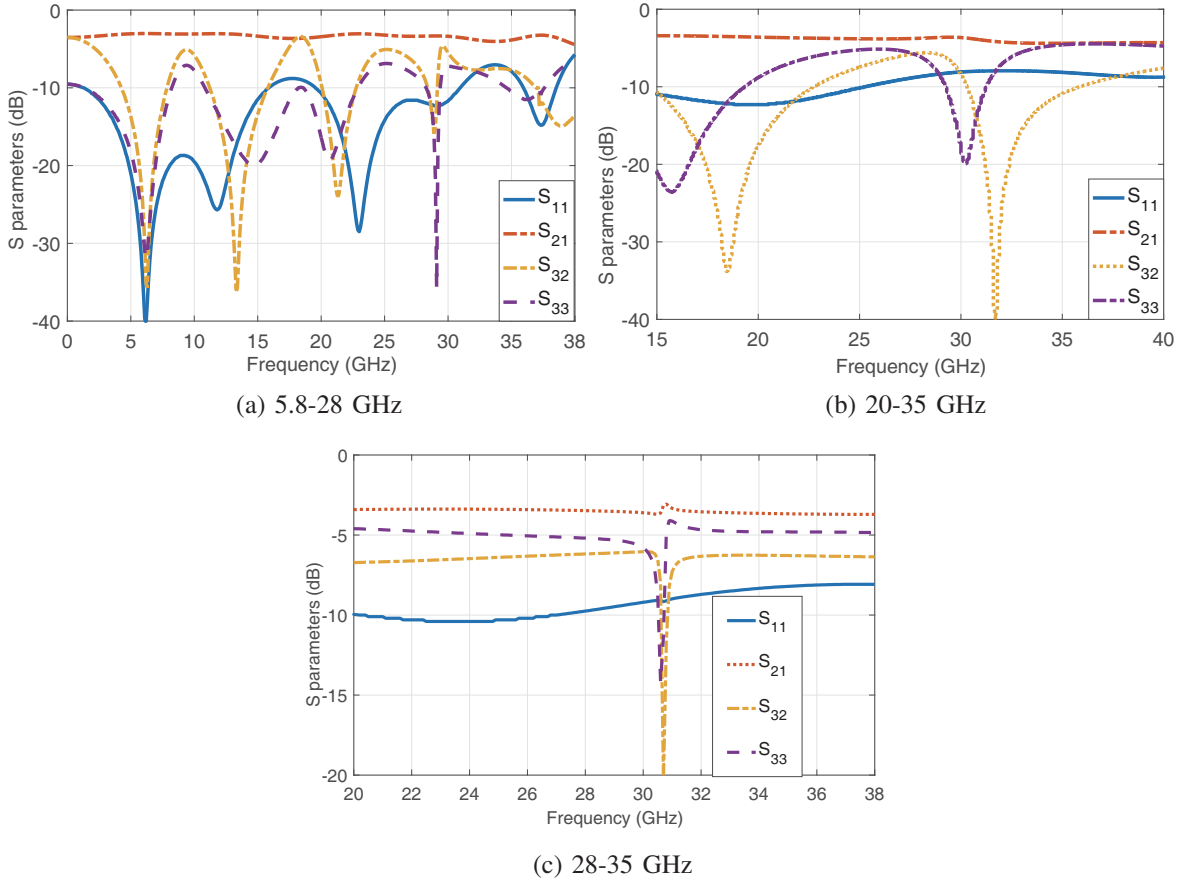
(a) 5.8-28 GHz

(b) 20-35 GHz

(c) 28-35 GHz

Figure 5. Design with packaging (a) 2.4–5.8 GHz, (b) 5.8–28 GHz, (c) 20–35 GHz, (d) 28–35 GHz.

the simulation shows acceptable results at the first frequency (5.8 GHz), but the results around 28 GHz are not similar to that of Figure 3(b). Clearly, the packaging affected the design. Also, it is noticeable that capacitor and inductor values (Table 1) are too small and that their availability is uncertain in the market for the second frequency (28 GHz). The simulation results shown in Figures 3(c) and (d) demonstrate the influence of the packaging effects and the difficulty to design an mm-wave component using capacitor and inductor and without taking the integration-related effects into consideration.

3. PROPOSED DESIGN

A schematic diagram of the proposed Wilkinson power divider, which realizes an equal power division at two arbitrary frequencies, is shown in Figure 6. The RLC lumped elements are substituted by only resistor r and transmission line with the characteristic impedance of Z_3 and Z_4 and the length of l_3 and l_4, respectively. The power divider is symmetric and we can, therefore, use the even-odd mode analysis to determine the circuit parameters for the dual-frequency power divider.

3.1. Even Mode

From Figure 7, even-mode analysis, and consider that the open circuit at f_1 and f_2, should be conserved after the transformer:

$$-jZ_4 \cot(\beta\ell_4) = jZ_3 \cot(\beta\ell_3) \tag{9}$$
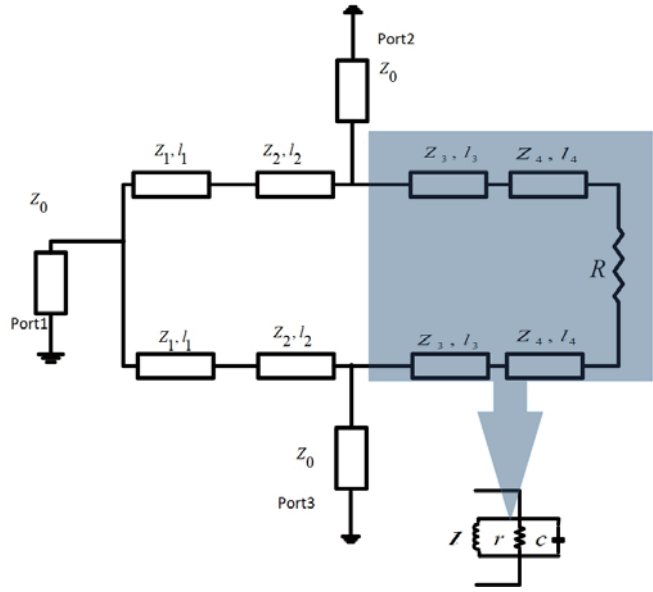
which define Z_3 as:

Figure 6. Proposed version with resistance and two additional transmission lines.
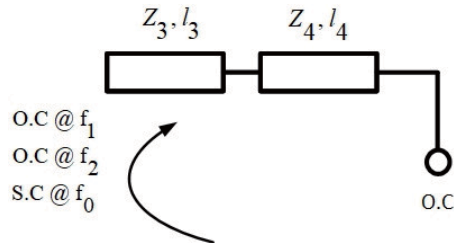

Figure 7. Even-mode analysis.

$$Z_3 = -Z_4 \frac{\tan(\beta\ell_3)}{\tan(\beta\ell_4)} \tag{10}$$

where n_1 and n_2 are arbitrary integers. At f_1 we can write:

$$\beta_1\ell_3 + \beta_1\ell_4 = n_1\pi \tag{11}$$

and at f_2:

$$m\beta_1\ell_3 + m\beta_1\ell_4 = n_2\pi \tag{12}$$

The two last equations support solution with:

$$\ell_3 = \frac{n_1\pi}{\beta_1 + \beta_2} \tag{13}$$

$$\ell_4 = \frac{n_2\pi}{\beta_1 + \beta_2} \tag{14}$$

At f_0, to ensure the out of band exclusion, the open circuit at f_0 should be transformed to a short circuit:
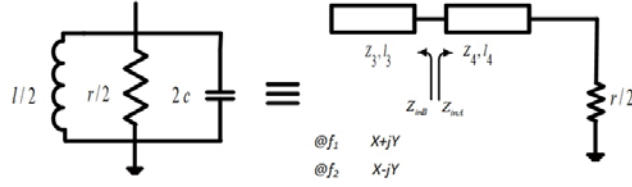
Figure 8. Odd-mode analysis.

$$\beta_0 \ell_3 + \beta_0 \ell_4 = (2p+1)\frac{\pi}{2} \tag{15}$$

We introduce the values of l_3 and l_4 from Eqs. (13) and (14) in Eq. (15):

$$\frac{\beta_0 n_1 \pi}{\beta_1 + \beta_2} + \frac{\beta_0 n_2 \pi}{\beta_1 + \beta_2} = \left(\frac{(2p+1)\pi}{2}\right) \tag{16}$$

$$\frac{n_1 \pi}{2} + \frac{n_2 \pi}{2} = \frac{(2p+1)\pi}{2} \tag{17}$$

$$n_1 + n_2 = (2p+1) \tag{18}$$

3.2. Odd-Mode Analysis

From Figure 8, the input impedances of the two-section Z_3, Z_4 transmission lines are given by

$$Z_4 \frac{\dfrac{R_L}{2} + jZ_4 \tan(\beta\ell_4)}{Z_4 + j\dfrac{R_L}{2}\tan(\beta\ell_4)} = Z_3 \frac{X + jY - jZ_3 \tan(\beta\ell_3)}{Z_3 - jX\tan(\beta\ell_3) + Y\tan(\beta\ell_3)} \tag{19}$$

X and Y represent the real and imaginary parts of the impedance of the half RLC circuit at f_1. Then the equations are attained by separating the real and imaginary parts. The real part is:

$$\frac{R_L}{2}Z_3 Z_4 + XZ_4^2 \tan(\beta\ell_3)\tan(\beta\ell_4) + Y\frac{R_L}{2}Z_4 \tan(\beta\ell_3)$$
$$= XZ_3 Z_4 - Y\frac{R_L}{2}Z_3 \tan(\beta\ell_4) + \frac{R_L}{2} * Z_3^2 \tan(\beta\ell_3)\tan(\beta\ell_4) \tag{20}$$

and the imaginary part is:

$$XZ_3 Z_4^2 \tan(\beta\ell_4) + YZ_4^2 \tan(\beta\ell_3)\tan(\beta\ell_4) - X\frac{R_L}{2}Z_4 \tan(\beta\ell_3)$$
$$= YZ_3 Z_4 - Z_3^2 Z_4 \tan(\beta\ell_3) + X\frac{R_L}{2}Z_3 \tan(\beta\ell_4) \tag{21}$$

Incorporating Eq. (10) in the real part gives.

$$-\frac{R_L}{2}\tan(\beta\ell_3) + X\tan(\beta\ell_3)\tan(\beta\ell_4)^2 + X\tan(\beta\ell_3) - \frac{R_L}{2}\tan(\beta\ell_3)^3 = 0 \tag{22}$$

The final equation of R_L is:

$$\frac{R_L}{2} = \frac{X}{2}\frac{1 + \tan(\beta\ell_4)^2}{1 + \tan(\beta\ell_3)^2} \tag{23}$$

Repeat the same elimination process by using Eq. (10) in the imaginary part to get Z_4:

$$-Z_4^3 + YZ_4^2 \tan(\beta\ell_4) - X\frac{R_L}{2}Z_4 = -YZ_4^2 \frac{1}{\tan(\beta\ell_4)} - Z_4^3 \frac{\tan(\beta\ell_3)^2}{\tan(\beta\ell_4)^2} - X\frac{R_L}{2}Z_4 \tag{24}$$

The final equation for Z_4 is

$$Z_4 = Y \frac{\tan(\beta\ell_4)^3 + \tan(\beta\ell_4)}{\tan(\beta\ell_4)^2 - \tan(\beta\ell_3)^2} \tag{25}$$

3.3. Frequency Ratio Parametric Study

Using Equations (25)–(23), (10), (13), and (14), the transmission lines length solutions (defined by n_1 and n_2) and impedance Z_3 and Z_4 are estimated for different frequency ratios of m. The value of Z_0 is considered $50\,\Omega$. The realizable microstrip line impedance values are fixed between 15 and $150\,\Omega$. To unravel Eqs. (14) and (15), the arbitrary integer values n_1 and n_2 are determined to be $n_{1,2} \in \{1, 2, 3, 4, 5, 6, 7, 8\}$, $n_1 \neq n_2$ (from 25) where the absolute value of $\tan(\beta\ell_3) \neq \tan(\beta\ell_4)$.

In study result illustrated in Figures 9(a) and 9(b), the out of band rejection is not considered. As can be seen in Figure 9(a), the minimal $n_1 + n_2$ satisfying the design rules fellow the ceiling pattern m.

$$n_1 + n_2 = \lceil m \rceil + 1.$$

$$n_1 + n_2 = \lceil 2m \rceil + 2.$$

and

$$n_1 + n_2 = \lceil 3m \rceil + 3. \tag{26}$$

Different possible values are also applicable giving more flexibility in the final framework. The equations are illustrated in Figure 9(a). In Figure 9(b), the graph shows that all the frequency ratios m are covered, and m values from 1 to 8 (except 2 and 3) could be represented by Z_3 and Z_4 values in a specified range, allowing for the widening of parameter choices covering more frequencies. The frequency ratio 2 and from 2.8 and 3 are not achievable due to harmonic singularity. However, the conventional WPD covers
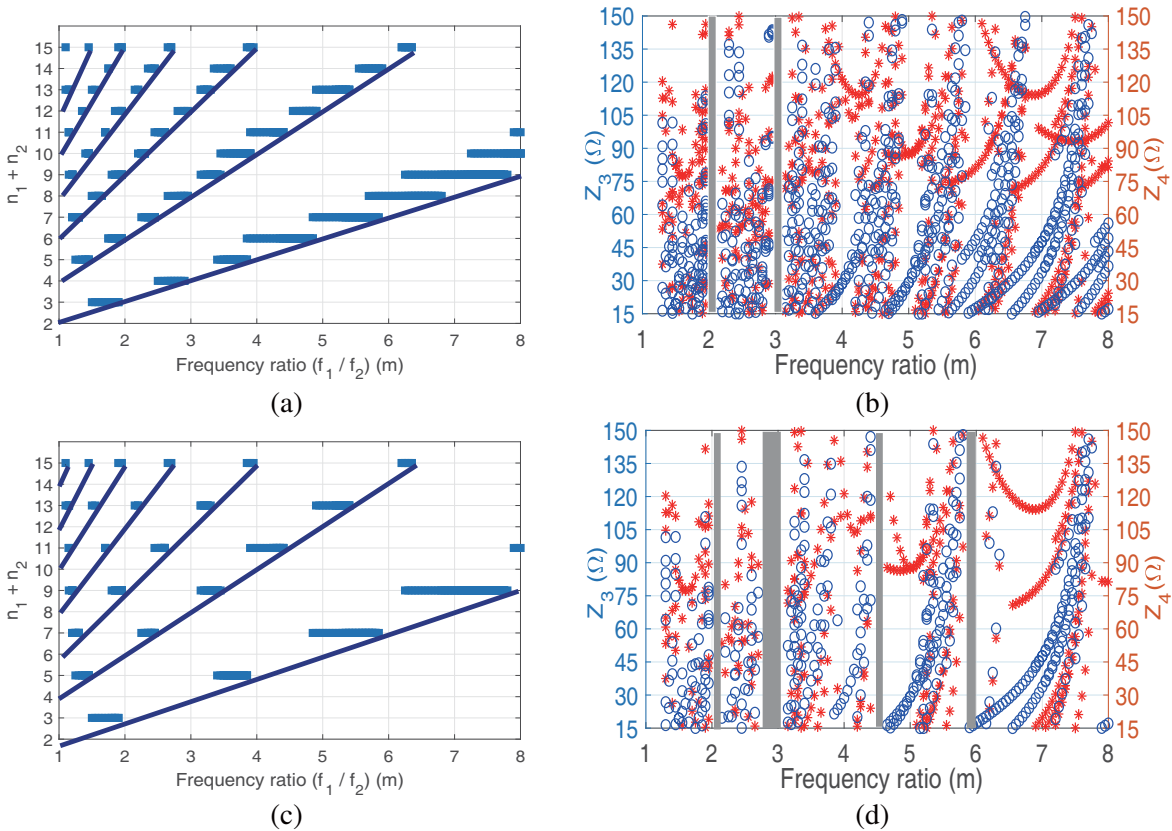

Figure 9. Parametric study of the proposed design (a) $n_1 + n_2$ with out $p + 1$. (b) $p + 1$. (c) $n_1 + n_2$ with $p + 1$. (d) with $p + 1$.

the third harmonic region ($m = 3$). Figures 9(c) and 9(d), demonstrate the application of the $2p + 1$ condition in addition to the previous conditions applied for Figures 9(a) and 9(b) to enhance the out of band rejection. In addition to the ratio around 2 and 3, we observe two other regions at 4.5 to 4.8 GHz, and 5.9 to 6.1 GHz where feasibility of Z_3, Z_4 values are less or over obtainable condition. In these two regions, it is possible to use Z_0 different from $50\,\Omega$ to reach feasible width. The $n1 + n2$ is defined by the same Eq. (26) with the consideration of odd value. Table 2 represents the values calculated using defined rules of the proposed design. Those values are used to simulate three sets of frequency using ADS. Table 3 summarizes the performance of the initial (Considering results from Figure 3) and proposed design. At 5.8–28 GHz, the initial design provides larger bandwidth at both frequencies.

Table 2. Proposed design transmission line parameters.

Frequency	$Z_3\,\Omega$	$Z_4\,\Omega$	θ_3	θ_4	$R_L\,\Omega$	n_1	n_2
5.8–28	33.79	55.2	138.4	55.3	118	5	2
20–35	47.6	90.3	130.9	65.45	144	2	1
28–35	23.7	49	320	240	15	4	3

Table 3. Frequency design bandwidth comparison.

Design	Initial (%)		Proposed (%)	
	f_1 GHz	f_2 GHz	f_1 GHz	f_2 GHz
5.8–28 GHz	5.2–6.3 6.5%	27.4–28.6 7.1%	5.5–6.1 3.5%	27.7–28.3 3.5%
20–35 GHz	18.8–21.1 8.3%	33.7–36.5 10.1%	18–21.9 14.1%	33.2–37 13.8%
28–35 GHz	28.2–28.6 1.2%	35.5–35.8 1.9%	27.7–28.2 1.5%	34.8–35.3 1.5%

The bandwidth results in the second frequency (20–35 GHz) depict different outcomes between the initial and proposed design. The second design outweighs the original model. The Third frequency set (28–35 GHz) presents equality in the results of both designs. Overall, it can be observed that the results of the proposed design converge for each dual frequency, and the achieved results of the proposed topology show the same bandwidth around the two frequencies.

3.4. Proposed Design Rules

The flowchart illustrated in Figure 10 summarizes the steps to design DBWPD starting from the desired two frequencies and input impedance. The steps followed are stated as:

- Using Eqs. (4), (3), and (1) to get Z_1, Z_2, θ_1, and θ_2 values with adequate n as detailed in Section 2.2.
- Calculate C, L, and R values from Eqs. (7) and (8).
- Assign arbitrary n_1 and n_2 values where $n_{1,2} \in \{1, 2, 3, 4, 5, 6, 7, 8\}$.
- $n_1 \neq n_2$ and $(n_1 \bmod n_2) \neq 0$ to ensure enhanced out of band performance. For some ratios, this enhancement is not feasible.
- Determine θ_3 and θ_4 from Eqs. (14) and (15).
- Calculate the values of Z_3, R_L, and Z_4 from Eqs. (10), (25), and (23), respectively.
- Confirm that R_L, Z_3, and Z_4 values are realizable according to the used substrate and available fabrication process limits.
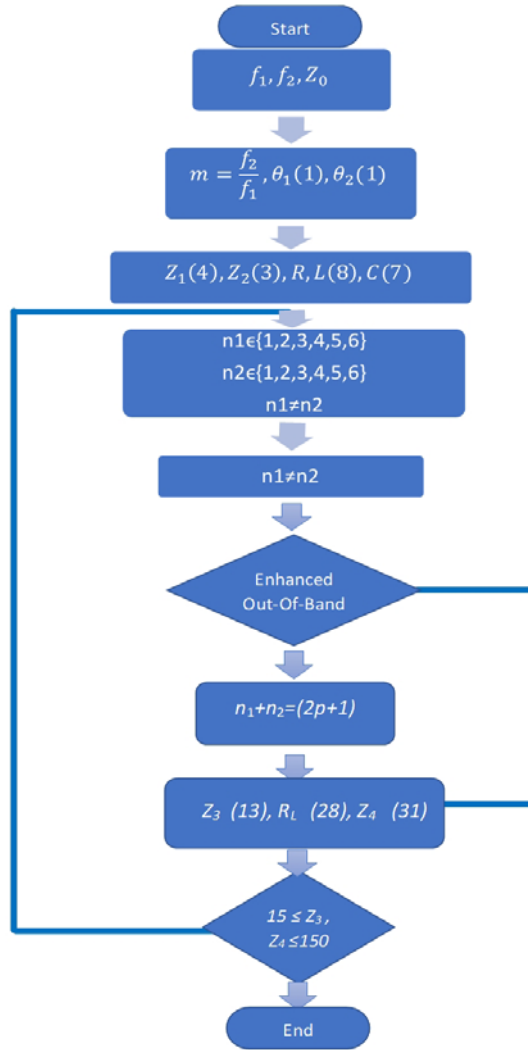
Figure 10. Parametric study flowchart.

4. EXPERIMENTAL RESULTS

To validate the proposed concept, different dual-band power dividers are designed operating at various dual-frequencies. The dual-band Wilkinson dividers have been fabricated on a 0.254 mm thick RO6002 substrate with relative permittivity of 2.95 and conductor thickness of 17 μm. Three power dividers have been designed. The first is for 5.8–35 GHz, the second for 20–35 GHz, and the third for 28-35 GHz. The simulation and optimization are completed by Ansoft HFSS 15.0.

Table 4 represents the dimension values of the design dimension shown in Figure 11. Photographs of fabricated power divider are represented in Figures 12(a), 12(b), and 12(c). 5.8–28 GHz illustrated in Figure 12(a). has an area of 1.8×2.9 cm^2. Through-Reflect-Load (TRL) calibration was used with two ports VNA to avoid the connector effects.

Figure 12(b) depicts the second Wilkinson power divider with a dimension of 1.3×1.2 cm^2. Figure 12(c) shows the third Wilkinson power divider with a dimension of 1.2×1.7 cm^2.

The design simulation and measurement results for the provided dual-band Wilkinson power dividers are shown in Figure 13. The simulated and measured insertion losses $|S_{21}|$ and $|S_{31}|$ are shown in Figures 13(a), 13(c), 13(e), and the return losses $|S_{11}|$ are illustrated in Figures 13(b), 13(d), 13(f) with the isolation $|S_{32}|$. The depicted results illustrate the agreement between simulated and measured results.

Table 4. Different designs dimensions.

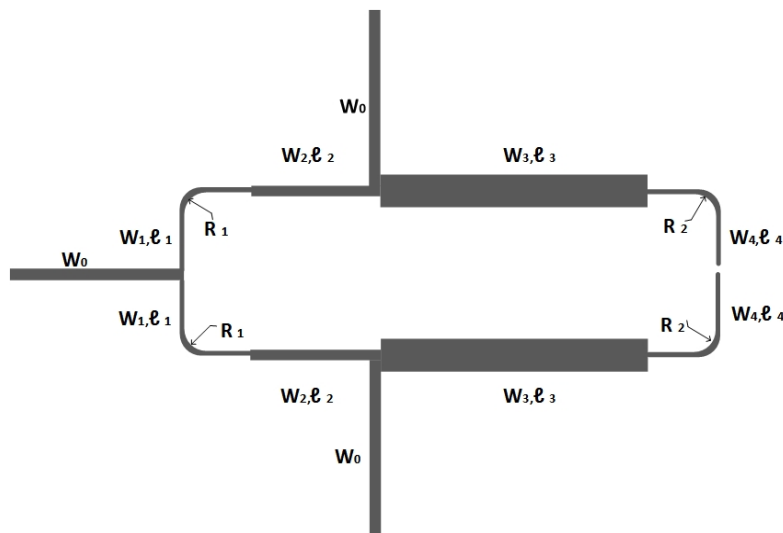| Frequency	5.8–28 GHz	20–35 GHz	28–35 GHz
W_0	13.4 mil	24.5	24.5
W_1	4.2 mil	7.2 mil	5 mil
W_2	7.3	15.6	8.9
W_3	75.2	27.3	44.3
W_4	10.1	6.9	14.2
L_1'	153.7	37.1	54.9
$L_1"$	37.4	11.2	101.9
L_2	238.6	73.3	62.3
L_3	526.5	126.7	223.7
L_4 R	$L_1' + L_1''$ 261.9 Ohm	$L_1' + L_1'' - 36$ 144 Ohm	$L_1' + L_1'' - 14.2$ 35.8 Ohm

Figure 11. Design dimensions.
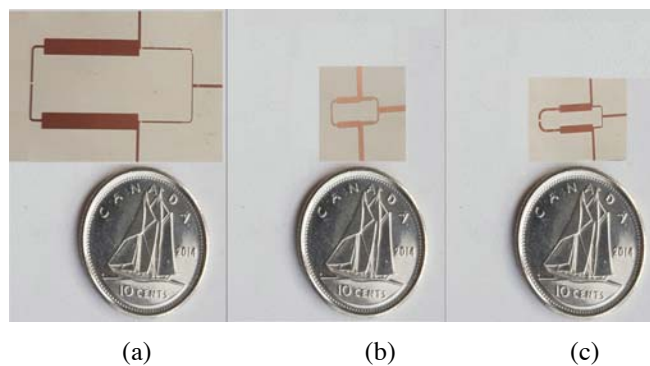
Figure 12. (a) 5.8–28 GHz photograph. (b) 20–35 GHz photograph. (c) 28–35 GHz photograph.

(a) 5.8-28GHz

(b) 5.8-28GHz

(c) 20-35 GHz

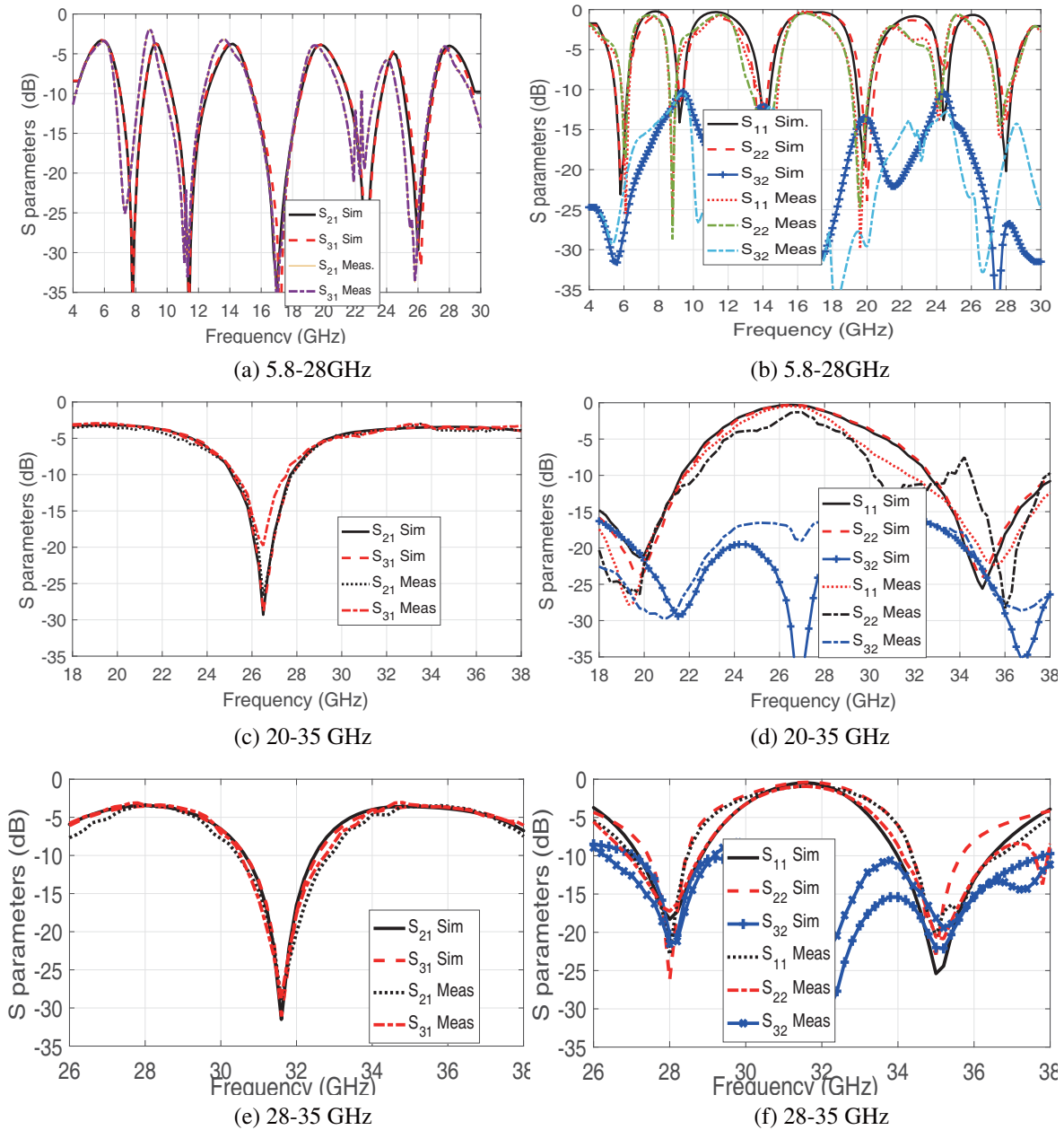(d) 20-35 GHz

(e) 28-35 GHz

(f) 28-35 GHz

Figure 13. Simulation and measurement results of S-parameters. (a) 5.8–28 GHz transmission coefficient. (b) 5.8–28 GHz reflection coefficient, and isolation. (c) 20–35 GHz transmission coefficient. (d) 20–35 GHz reflection coefficient, and isolation. (e) 28–35 GHz transmission coefficient. (f) 28–35 GHz reflection coefficient, and isolation.

At the first set of two frequencies (5.8–28 GHz), as shown in Figure 13(a)(b), in the simulation, insertion losses of 3.4 and 3.6 are observed at 5.8 and 28 GHz, respectively. The measured counterpart shows 3.4 dB and 3.8 dB. The 10 dB of matching occurs from 5.5 to 6.1 GHz and from 27.7 to 28.3 GHz in the simulation. Further, 5.5 to 6.2 GHz are depicted at 5.8 GHz and 27.7 to 28.3 at 28 GHz for the measurement. Simulation and measurement of reflection coefficient are shown in Figure 13(b), with 23 dB and 25 dB at 5.8 GHz and 20 dB, and 16 dB at 28 GHz, respectively. Isolation of more than 20 dB is achieved in the 10 dB matching bandwidth around 5.8 GHz and 28 GHz.

The second set of graphs shown in Figures 13(c) and 13(d) characterizes the dual-frequency 20–

35 GHz DBWPD performance. Simulation in Figure 13(c) presents an insertion loss of 3.4 dB at 20 GHz and 3.6 dB at 35 GHz. The measurement results demonstrate $|S_{21}|$ for the first frequency of 3.6 dB and 3.8 dB at 35 GHz, while the simulated reflection coefficient shows 4 GHz (18–21.8) of 10 dB matching at the first frequency and 6 GHz (31.9–38 GHz) at the second one. Meanwhile, the measurement results demonstrate matching bandwidths of 18 to 21.7 at 20 GHz and 31 to 38.8 GHz at 35 GHz. The 20 dB isolation bandwidths are from 19.9 to 23.5 at 20 GHz and 34 to 38.5 at 35 GHz.

The last set of graphs at dual-frequency 28–35 GHz is represented in Figures 13(e) and 13(f). Simulation results depict transmission coefficients of 3.55 dB at 28 GHz and 3.6 dB at 35 GHz. Measurement shows 3.3 dB at 28 GHz and 3.2 dB at 35 GHz. Return loss referenced 10 dB matching is achieved at both frequencies for each of the simulation (27.7 to 28.2 GHz and 34.8 to 35.3 GHz) and measurement results (27.4 to 28.4 GHz and 34.4 to 35.6 GHz). Simulated isolation is shown in Figure 13(f) which depicts about 20.2 dB for 28 GHz and 22 dB at 35 GHz. $|S_{32}|$ measurement represents 20 dB at the first frequency and 19.2 dB at the second band. The out of band rejection performance is enhanced at the new design compared to that in the initial counterpart.

Table 5 presents comparisons of symmetrical dual-band WPD designs in terms of frequencies, frequency ratio, bandwidth, and out-of-band rejection (OBR). The bandwidth is referenced to the 10 dB $|S_{11}|$. The (OBR) demonstrates $|S_{11}|$ and $|S_{22}|$ at the center frequency ($\frac{f_1+f_2}{2}$) to show the rejection. It is clear that the proposed WPD is the design with frequencies in the millimeter wave bands. Its bandwidth results present equality at both frequencies in all the proposed designs, and their OBR indicates good rejection.

Table 5. Comparison With previous designs.

Ref	Freq (GHz)	Design	Bandwidth	Freq. ratio	OBR (dB)		
					$S11$	$S22$	$S21$
2	1–1.8	2 TL+RLC	20%–28.5%	1.4	−20	−6	−3.2
2	1–4	2 TL+RLC	2%–6%	2.5	−10	−10	3.8
6	1–2.6	2TL+1CS/OSTL+R	22.2%–8%	1.8	−5	−19	−5.5
8	1–2	*TL+parallel LC	30.1%–7%	1.5	−22	−10	3.25
10	0.9–2.45	CRLH* Stub	11.9%–8%	1.675	−2	−7	20
11	1–3.5	5TLs+1R	50%–15%	2.25	−2	−5	−5.8
11	1–3.5	5TL+2OC+1R	44.6%–5%	2.25	−1	−2.5	−23.8
This work	5.8–28	4 TL+R	3.5%–3.5%	4.8	0	0.2	−27
	20–35	4 TL+R	14.1%–13.8%	1.75	0	0.2	−23
	28–35	4 TL+R	1.5%–1.5%	1.25	−1	−0.5	−20

* CRLH=composite right-/left-hand TL

5. CONCLUSION

A dual-band Wilkinson power divider for a millimeter-wave integrated circuit with out-of-band rejection capability is proposed and realized. The design proposes the replacement of the RLC circuit with transmission lines and a resistor, thereby reducing the cost and complexity while enhancing the performance. The layout equations are derived and demonstrated. The range of lower and upper band frequency ratios is studied from 1 to 8. Good agreement between simulated and measured results is perceived. Moreover, the design exhibits good out-of-band rejection performance and also the equalization of bandwidth percentage around the two-band. A future design could consider substituting the lumped element resistor with a thin-film resistor to enhance the performance.

ACKNOWLEDGMENT

REFERENCES

1. Deng, P.-H., J.-H. Guo, and W.-C. Kuo, "New Wilkinson power dividers based on compact stepped-impedance transmission lines and shunt open stubs," *Progress In Electromagnetics Research*, Vol. 123, No. November 2011, 143–158, 2012.

2. Park, M.-J. and B. Lee, "A dual-band Wilkinson power divider," *IEEE Microw. Wirel. Components Lett.*, Vol. 18, No. 2, 85–87, 2008.

3. Cheng, K.-K. and F.-L. Wong, "A new Wilkinson power divider design for dual band application," *Microw. Wirel. Components Lett. IEEE*, Vol. 17, No. 9, 664–666, 2007.

4. Osseiran, A., J. F. Monserrat, P. Marsch, M. Dohler, and T. Nakamura, *5G Mobile and Wireless Communications Technology*, Cambridge University Press, 2016.

5. Ericsson, "5G deployment considerations in today s networks," Tech. Rep., Ericsson.com, 2018.

6. Gómez-García, R., R. Loeches-Sánchez, D. Psychogiou, and D. Peroulis, "Single/multi-band Wilkinson-type power dividers with embedded transversal filtering sections and application to channelized filters," *IEEE Trans. Circuits Syst. I Regul. Pap.*, Vol. 62, No. 6, 1518–1527, 2015.

7. Lin, Y. S. and C. Y. Lin, "Miniature dual-band quadrature coupler with arbitrary power division ratios over the two bands," *IEEE Trans. Circuits Syst. I Regul. Pap.*, Vol. 67, No. 2, 634–646, 2020.

8. Cheng, K.-K. M. and C. Law, "A novel approach to the design and implementation of dual-band power divider," *IEEE Microwave Theory and Techniques*, Vol. 56, No. 2, 473–476, 2008.

9. Wang, X., I. Sakagami, K. Takahashi, and S. Okamura, "A generalized dual-band Wilkinson power divider with Parallel L, C, and R components," *IEEE Trans. Microw. Theory Tech.*, Vol. 60, No. 4, 952–964, 2012.

10. Wu, L., Z. Sun, H. Yilmaz, and M. Berroth, "A dual-frequency Wilkinson power divider," *Microw. Theory Tech. IEEE Trans.*, Vol. 54, No. 1, 278–284, 2006.

11. Horst, S., R. Bairavasubramanian, M. M. Tentzeris, and J. Papapolymerou, "Modified Wilkinson power dividers for millimeter-wave integrated circuits," *IEEE Trans. Microw. Theory Tech.*, Vol. 55, No. 11, 2439–2445, 2007.

12. Zhao, M., A. Kumar, C. Wang, B. Xie, T. Qiang, and K. K. Adhikari, "Design method of dual-band Wilkinson power divider with improved out-of-band rejection performance and high design exibility," *AEU — Int. J. Electron. Commun.*, Vol. 110, 152844, 2019.

13. Monzon, C., "A small dual-frequency transformer in two sections," *IEEE Trans. Microw. Theory Tech.*, Vol. 51, No. 4 I, 1157–1161, 2003.

14. Antsos, D., R. Crist, and L. Sukamto, "A novel Wilkinson power divider with predictable performance at K and Ka-band," *IEEE MTT-S Digest*, 907–910, 1994.

15. Garg, R. and I. Bahl, "Characteristics of coupled microstriplines," *IEEE Trans. Microw. Theory Tech.*, Vol. 27, No. 7, 700–705, 1979.